Vibrational Properties of a Monolayer Silicene Sheet Studied
by Tip-Enhanced Raman Spectroscopy

Shaoxiang Sheng,[1] Jiang-bin Wu,[2] Xin Cong,[2] Wenbin Li,[1] Jian Gou,[1] Qing Zhong,[1]
Peng Cheng,[1] Ping-heng Tan,[2,3,*] Lan Chen,[1] and Kehui Wu[1,3,4,†]

[1]*Institute of Physics, Chinese Academy of Sciences, Beijing 100190, China*
[2]*State Key Laboratory of Superlattices and Microstructures, Institute of Semiconductors,
Chinese Academy of Sciences, Beijing 100083, China*
[3]*School of physical sciences, and College of Materials Science and Opto-Electronic Technology,
University of Chinese Academy of Sciences, Beijing 100049, China*
[4]*Collaborative Innovation Center of Quantum Matter, Beijing 100871, China*

Combining ultrahigh sensitivity, spatial resolution, and the capability to resolve chemical information, tip-enhanced Raman spectroscopy (TERS) is a powerful tool to study molecules or nanoscale objects. Here we show that TERS can also be a powerful tool in studying two-dimensional materials. We have achieved a 10^9 Raman signal enhancement and a 0.5 nm spatial resolution using monolayer silicene on Ag(111) as a prototypical 2D material system. Because of the selective enhancement on Raman modes with vertical vibrational components in TERS, our experiment provides direct evidence of the origination of Raman modes in silicene. Furthermore, the ultrahigh sensitivity of TERS allows us to identify different vibrational properties of silicene phases, which differ only in the bucking direction of the Si-Si bonds. Local vibrational features from defects and domain boundaries in silicene can also be identified.

Introduction.—Silicene is a two-dimensional (2D) honeycomb lattice that consists of silicon atoms, which can be regarded as the silicon version of graphene. The electronic band structure of silicene hosts Dirac fermions [1–3], giving rise to the theoretically predicted quantum spin Hall effect and possible spintronic applications, which are of great interest to the silicon industry [4,5]. The structures and electronic proprieties of silicene have been extensively studied in the last few years. However, the vibrational properties of silicene still remain largely elusive, partially because *ex situ* optical spectroscopy characterizations are hampered by the oxidation of silicene in ambient condition. So far, only a few *in situ* Raman spectroscopy studies have been reported [6–8]. These measurements, however, failed to distinguish different phases of silicene when they coexist on the surface. In addition, as the integration of Raman spectroscopy into ultrahigh-vacuum (UHV) systems usually results in low efficiency, the spectroscopy quality remains to be improved.

Compared with normal Raman, scanning tunneling microscopy (STM) with tip-enhanced Raman spectroscopy (TERS) utilizes the atomically sharp STM tip to enhance the Raman signal. The signal enhancement factor can be as high as 10^8 [9]. Recently, improvements in the spatial resolution, down to the subnanometer scale, have been demonstrated in the "gap-mode" (both tip and substrate are plasmonic metals, such as Au/Ag) TERS on carbon nanotubes [9] and molecules on Ag(111) surfaces [10,11]. With such a high spatial resolution, it is possible to study the local vibrational properties of silicene *in situ* in ultrahigh vacuum.

In the present work, we demonstrate a high-performance TERS spectroscopy based on a UHV low-temperature STM system. A signal enhancement factor as high as 10^9 and a TERS spatial resolution of 0.5 nm have been achieved by using silicene on Ag(111) as a prototypical system. As such, we were able to distinguish the vibrational signatures of different monolayer silicene phases, which are different only in the buckling direction of the Si-Si bonds. Moreover, the TERS enhancement is phonon mode selective, which helps us to clarify the origins of the Raman peaks of silicene. The subnanometer spatial resolution also makes it possible to distinguish the Raman signatures from defects and domain boundaries in silicene. This work paves the way to employ TERS as a universal, high-sensitive local tool to study emerging new 2D materials.

Method.—Our TERS is built in a homemade LT-UHV STM system, with side illumination and backscattering collection configuration, as shown in Fig. 1(a). The aspheric lens (NA = 0.42, f = 24 mm, diameter = 25 mm) inside the STM body can be adjusted by a 3D piezoelectric motor. The Ag(111) surface was prepared by standard cycles of argon ion sputtering and annealing at about 800 K. Silicene was prepared by heating a Si wafer piece ($T \sim 1300$ K) to evaporate Si onto the Ag(111). A chemically etched silver tip was used for TERS measurements and STM imaging. A single longitudinal mode fiber coupled cw laser (Cobolt, Sweden) was used to provide a *p*-polarized laser light as the Raman pumping source, with the wavelength at 532 nm and a photon flux about 10 kW/cm². The scattered Raman signals were dispersed
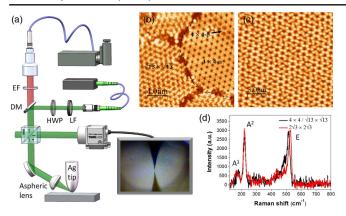
FIG. 1. The experimental setup. (a) Schematic of LT-UHV STM based TERS setup. EF: edge filter, DM: dichroic mirror, HWP: half wave plate, LF: laser line filter. (b), (c) Atomic resolution STM topography of coexisted 4×4 and $\sqrt{13} \times \sqrt{13}$ [(b), 0.2 V, 300 pA], and $2\sqrt{3} \times 2\sqrt{3}$ [(c), 2 V, 50 pA] silicene phase. (d) Corresponding *in situ* normal Raman spectra (Laser power is about 5 mW, acquisition time is 600 s).

by a 1200 grooves/mm grating and collected by a liquid nitrogen cooled charge coupled device (CCD) (Princeton Instrument, SP2300i). All TERS experiments were carried out at a sample temperature of 77 K, and a base pressure around 2×10^{-10} mbar.

The phonon spectra and vibrational density of states (VDOS) were calculated using density functional perturbation theory (DFPT) implemented in the Quantum Espresso code [12]. For the calculation of the phonon dispersion of silicene on Ag(111), VASP [13] and PHON [14] were used, with exchange-correlation potential described by the Perdew-Burke-Ernzerhof (PBE) function [15]. The cutoff energy of the plane wave was 360 eV, and Monkhorst-Pack [15] reciprocal grids is $12 \times 12 \times 1$. The structure of the (3×3) and $\sqrt{7} \times \sqrt{7}$ silicene supercells are relaxed on a 5 layers Ag(111) substrate. In the phonon dispersion calculation by PHON, only the silicene part was considered, by using the same isolated method in Ref. [6].

Results and discussions.—Si-Si bonds in silicene exhibit various buckling configurations on Ag(111) surface, resulting in ordered phases, such as 4×4 (silicene 3×3 supercell on Ag(111) 4×4 supercell), $(\sqrt{13} \times \sqrt{13})R13.9°$ (silicene $\sqrt{7} \times \sqrt{7}$ on Ag(111) $\sqrt{13} \times \sqrt{13}$), and $(2\sqrt{3} \times 2\sqrt{3})R30°$ (silicene $\sqrt{7} \times \sqrt{7}$ on Ag(111) $2\sqrt{3} \times 2\sqrt{3}$) [16–18]. The 4×4 and $\sqrt{13} \times \sqrt{13}$ phases usually coexist [Fig. 1(b)], whereas the $2\sqrt{3} \times 2\sqrt{3}$ phase can be prepared as a single phase covering the entire Ag(111) surface [Fig. 1(c)] [18]. We first obtained the far field Raman spectra (without tip enhancement) for a mixed $4 \times 4 / \sqrt{13} \times \sqrt{13}$ surface and a pure $2\sqrt{3} \times 2\sqrt{3}$ surface, respectively, as shown in Fig. 1(d). Three major peaks are presented in the spectra, which agree with the *in-situ* Raman measurement by D. Solonenko *et al.* [6]. The peak around 520 cm^{-1} ($4 \times 4 / \sqrt{13} \times \sqrt{13}$ at 515 cm^{-1}, and

$2\sqrt{3} \times 2\sqrt{3}$ at 527 cm^{-1}) is known as the E mode, corresponding to a double-degenerated modes of the in-plane transversal optical (TO) and in-plane longitudinal optical (LO) phonon branches [19]. It has been observed in both *in situ* and *ex situ* Raman studies [20]. The presence of the E mode reflects the honeycomb nature of 2D silicene. The two low energy modes, at around 170 and 218 cm^{-1}, are only reported by *in situ* Raman measurements [6,7] and are absent in *ex situ* measurements [20]. The peak at 218 cm^{-1} was also not presented in the calculated phonon spectrum of freestanding silicene [19], it had been suggested to be Raman bands activated by defects (analogy to the so-called D band in graphene) [7]. Recently, D. Solonenko *et al.* determined from the polarization dependence of these peaks that they should be phonon modes with A symmetry [6]. Here, we denoted these modes as A^1 and A^2 modes following Ref. [6].

When the STM tip is brought close to the silicene surface, strong enhancement of the Raman signal is observed, as shown in Fig. 2(a). Both the A^1 and A^2 peaks exhibit dramatic tip-enhancement and become the dominant peaks as the tip is close to the surface. In contrast, the E mode shows negligible enhancement and becomes insignificant when the tip is close to the surface. This phenomenon can be understood as the tip mainly enhances the vertical electric field along the tip axis, so only the out-of-plane vibrational modes are enhanced [10]. The A modes have dominating out-of-plane vibration of the Si atoms; thus, they can be effectively enhanced under a local vertical electric field. In contrast, in the E mode, the displacements of Si atoms are purely in-plane, so it exhibits negligible tip enhancement under a vertical electric field. This selection rule can be expressed by the TERS intensity of each mode, $I_{\text{TERS},M} \propto |\alpha_{ZZ,M} g_{zz}^2|^2$, where g_{zz} is the ZZ component of the electric field enhancement tensor and $\alpha_{ZZ,M}$ is the ZZ component of the Raman tensor of each mode. Because both A^1 and A^2 modes have a nonzero α_{ZZ} Raman tensor [6], they can be effectively enhanced under a vertical electric field. In contrast, in the E mode, the α_{ZZ} Raman tensor is zero, so it exhibits negligible tip enhancement. Thus, our TERS experiment provides a direct support to the assignment of the major Raman peaks of silicene at 170 and 218 cm^{-1}, and 520 cm^{-1} to A^1, A^2, and E modes.

A careful calibration on the intensity of the A^1 mode as a function of the gap distance between the tip and the sample, as detailed in the Supplemental Material [21] which include Refs. [22–33], indicates that we have achieved an unprecedent TERS enhancement factor up to 10^9. The dependence of TERS intensity on the gap distance fits well with an exponential decay [Fig. 2(b)], suggesting that the TERS enhancement comes from the enhancement of the local electric field. Moreover, an extremely high TERS lateral spatial resolution were also demonstrated in the same system. As shown in Fig. 2(c), the flat area on the left side is the clean Ag surface, and the
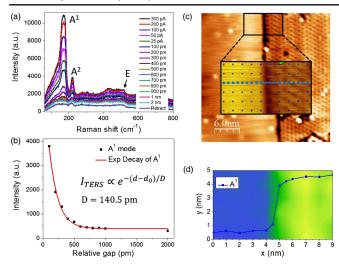
FIG. 2.   Enhancement factor and spatial resolution of TERS.
(a) Gap-distance dependent TERS spectra of silicene $\sqrt{13} \times \sqrt{13}$
phase (1 V, 50 s for each spectrum). (b) TERS intensity of the A^1
mode dependent on the relative gap distance (tip retracted from
100 pm to 2 nm. The TERS data with tunneling current were not
used, as the tip height is difficult to acquire with feedback on).
(c) STM topography of $\sqrt{13} \times \sqrt{13}$ phase on Ag(111) surface,
inset is the enlarged STM image in the black box. (d) A^1 mode
TERS intensity mapping of $\sqrt{13} \times \sqrt{13}$ phase on Ag(111)
surface in the inset in (c), the overlapped dots line is the A^1
mode TERS intensity along the blue dot line in (c) (1V, 300 pA).

right part is silicene with $\sqrt{13} \times \sqrt{13}$ phase. TERS spectra
were recorded along the blue dots line in the inset in
Fig. 2(c). The color map in Fig. 2(d) illustrates the chemical
distribution on the surface. When the tip moves across a
step, the Raman intensity (A^1 mode is used as the reference
peak) follows the abrupt morphology change, giving a
spectroscopic spatial resolution as high as 0.5 nm spatial
resolution with a 10%–90% contrast, which is among the
best record so far [10,11].

Because of the extremely high signal enhancement and
spatial resolution, we were also able to resolve vibrational
features that are not observable in normal Raman spec-
troscopy. Figures 3(a)–3(c) show the gap-distance depen-
dent TERS spectra of 4×4, $\sqrt{13} \times \sqrt{13}$, and $2\sqrt{3} \times 2\sqrt{3}$
phases, respectively, obtained by placing the STM tip on
top of each specific phase. In addition to the A^1, A^2, and E
peaks, several additional features can be observed, includ-
ing a side peak (LA) around 120 cm^{-1}, which results in the
asymmetric shape of the A^1 peak, and a serials of small
peaks, which can be classified into two groups, one around
300 cm^{-1} (denoted by ZO$_x$) and the other around
420–480 cm^{-1} (denoted by LO$_x$ and TO), respectively.
Note that these spectra were obtained locally from an
effective area of ∼1 nm size, which is guaranteed by high
resolution STM images to be clean silicene phases.
Therefore, we can safely rule out any contamination
induced peaks, such as those from amorphous silicon [34].

Carefully inspecting the TERS spectra of different
phases, one can notice the clear difference among them.
For examples, the spectrum of $2\sqrt{3} \times 2\sqrt{3}$ phase has a
much higher LA band, resulting in an apparently fatter A^1
peak. This may be explained by the fact the $2\sqrt{3} \times 2\sqrt{3}$
phase is more disordered, and thus the Raman selection
rules are more relaxed, allowing a more effective excitation
of the LA band. In addition, $2\sqrt{3} \times 2\sqrt{3}$ phase also
exhibits a broader LO-TO band; i.e., LO-TO peaks are
more split. In contrast, the ZO band is stronger and more
split in the spectrum of 4×4 phase, while it is weaker in
the spectrum of $2\sqrt{3} \times 2\sqrt{3}$ phase, and only slightly visible
in the spectrum of $\sqrt{13} \times \sqrt{13}$ phase.

These additional peak features, however, cannot be
explained without considering the substrate effect. In the
calculated phonon spectra of free-standing silicene with
3×3 and $\sqrt{7} \times \sqrt{7}$ reconstructions [with respect to sili-
cene 1×1, corresponding to 4×4 and $2\sqrt{3} \times 2\sqrt{3}$ phases
on Ag(111)], ZO and LO(TO) bands are presented in the
Brillouin zone center due to phonon folding in the super-
cell, but their energies are degenerated at the Γ point;
therefore, both ZO and LO should exhibit only single
narrow peaks. In order to reproduce the multiple peaks in
the ZO and LO bands, we included the Ag(111) substrate in
the calculation, as shown in Figs. 3(g)–3(i). The degen-
erated ZO, LO(TO) modes are found to split to multiple
phonon branches at the Γ point, agreeing well with our
experiment. Furthermore, the differences in the ZO and
LO-TO groups in different silicene phases can also be
perfectly reproduced in the calculated phonon spectra.
Firstly, in the measured spectrum of $2\sqrt{3} \times 2\sqrt{3}$ phase,
the LO mode is clearly redshift and split at ∼395 (LO$_1$) and
426 cm^{-1} (LO$_2$), whereas the LO-TO bands in 4×4 and
$\sqrt{13} \times \sqrt{13}$ are located in a narrower energy region, more
close to the E mode at 520 cm^{-1}. These features are
perfectly reproduced in the calculations. On the other hand,
the 4×4 phase exhibits apparently difference ZO group
compared with those of $2\sqrt{3} \times 2\sqrt{3}$ and $\sqrt{13} \times \sqrt{13}$
phases. There is a peak at ∼380 cm^{-1} (ZO$_3$) of 4×4
phase [Fig. 3(d)], which is absent in $\sqrt{13} \times \sqrt{13}$ and
$2\sqrt{3} \times 2\sqrt{3}$ phases [Figs. 3(e)–3(f)]. In the calculated
phonon spectrum [Fig. 3(g)], a ZO phonon branch reaches
exactly this energy at the Γ point, which is absent in the
phonon spectra of $2\sqrt{3} \times 2\sqrt{3}$ and $\sqrt{13} \times \sqrt{13}$ phases
[Figs. 3(h)–3(i)]. The atomic vibrational pictures of each
Raman modes are all summarized in Table S1 [21]. Note
that the low-frequency modes of LA, A^1, and A^2 have large
out-of-plane vibration components, which explains their
large TERS enhancement. On the other hand, the ZO, LO,
and TO modes have much smaller out-of-plane compo-
nents, correspondingly, their TERS enhancements are
much less significant. Note that the A^2 peak can also be
attributed to one phonon branch at Γ point which possesses
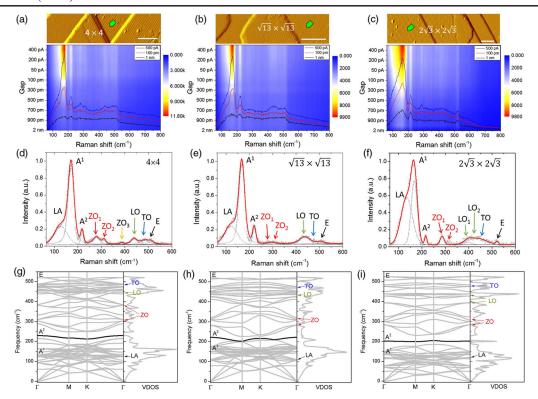
FIG. 3.   Near field Raman spectra of silicene and the calculated supercells phonon dispersion curves with taking into account the effect of Ag(111) substrate. (a)–(c) Gap-distance dependent TERS spectra map of silicene 4×4 (a) $\sqrt{13} \times \sqrt{13}$ (b) and $2\sqrt{3} \times 2\sqrt{3}$ (c) phases (1 V, 50 s), with tip position in the corresponding STM topography (upper panels, the scale bar is 10 nm). (d)–(f) Pure near field TERS spectra (subtracted far field signals) of silicene 4×4 (d), $\sqrt{13} \times \sqrt{13}$ (e), and $2\sqrt{3} \times 2\sqrt{3}$ (f) phases. Experimental data are shown by gray crosses, and the fitting data are plotted by red solid lines. Each single mode is plotted by dash gray line. (g)–(i) The supercells phonon dispersion curves and VDOS of the silicene 4×4 phase (g) $\sqrt{13} \times \sqrt{13}$ phase (h) and $2\sqrt{3} \times 2\sqrt{3}$ phase (i) epitaxial on Ag(111) surface.

the narrowest peak width, agreeing with our experiment [Figs. 3(a)–3(c)] and Ref. [6].

Finally, the ultrahigh sensitivity of TERS also allows us to study the local vibrational properties induced by defects or domain boundaries in silicene. The silicene T phase was rarely discussed in literature. It was likely a partially disordered phase consists incomplete silicon rings [18], and also suggested to be another type of $\sqrt{13} \times \sqrt{13}$ phase [16]. Here, our TERS results indicate significant differences between the TERS spectra of T phase compared with those from other ordered silicene phases, as shown in Fig. 4(a). It exhibits a blue shift of A^1 peak, and with a strong shoulder peak at 130 cm^{-1}. The A^2 peak is almost absent in T phase. It maybe because the relaxation of the Raman selection rule for LA mode due to the disorder of the silicon rings, and the A^2 mode is suppressed due to a very different silicene-Ag interaction as compared with other ordered phases.

It is known that another phase with a 4×4 periodicity, namely, $4 \times 4 - \beta$ phase, commonly exists at the boundary between different normal 4×4 domains (noted as $4 \times 4 - \alpha$ phase) [35,36]. The strain effect helps to stabilize the $4 \times 4 - \beta$ phase. The TERS spectra taken on $4 \times 4 - \alpha$ region and at the boundary (β phases) show clear differences. As shown in Fig. 4(d), the β phase shows a

slight redshift (~ 4 cm^{-1}) of the A^1 mode and a much lower peak at ZO peaks (280 and 310 cm^{-1}) compared with α phase. The TERS spectrum at the edge of a $4 \times 4 - \alpha$ domain was also measured, and its A^1 and A^2 peaks are similar like those of the $4 \times 4 - \beta$ phase but with an even lower intensity. Considering that the A^2 peak and the ZO peaks are directly related to the interaction between silicene and the substrate, the decreasing A^2 and ZO peak intensity from α, β to edge may imply decreasing interaction with the substrate due to strain relaxation at the domain boundary and domain edge, respectively.

In summary, we have demonstrated TERS with enhancement factor as high as 10^9, and spatial resolution of 0.5 nm using a 2D material silicene on Ag(111) as a model system. The vibrational fingerprints of different silicene phases, which differ only in the buckling direction of the Si-Si chemical bonds, can be distinguished in TERS spectra. In addition we have revealed ZO, LO, and TO phonon modes at high frequencies, which were not observable in normal Raman. We show that beyond molecules, TERS can also play powerful roles in studying 2D materials. The highly enhanced field perpendicular to the surface may also be a useful tool to tune the properties of 2D materials, such as to open an energy gap at K points [4,5] of silicene energy
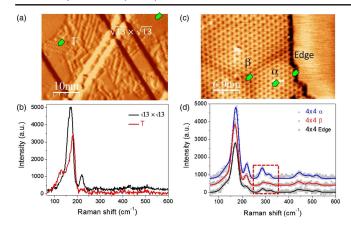
FIG. 4.   TERS spectra of silicene at defect, edge and local strain positions. (a) STM topography of coexisting silicene T phase and $\sqrt{13} \times \sqrt{13}$ phase. (b) TERS spectra of T phase and well-ordered $\sqrt{13} \times \sqrt{13}$ phase, with the tip at the corresponding position marked in (a) (1 V, 100 pA), shows very different spectra. (c) STM topography of silicene $4 \times 4 - \alpha$ phase and β phase. (d) TERS spectra at $4 \times 4 - \alpha$ phase, β phase, and domain edge, with the tip at the corresponding position in (c) (1 V, 50 pA). The far field signal has been subtracted from all of the TERS spectra, the acquisition time is 50 s, and the laser power is about 10 mW.

bands, which is potentially useful for the light controlled logic circuit.

---

[*]phtan@semi.ac.cn
[†]khwu@iphy.ac.cn

[1] B. J. Feng, H. Li, C. C. Liu, T. N. Shao, P. Cheng, Y. G. Yao, S. Meng, L. Chen, and K. H. Wu, ACS Nano **7,** 9049 (2013).
[2] L. Chen, H. Li, B. Feng, Z. Ding, J. Qiu, P. Cheng, K. Wu, and S. Meng, Phys. Rev. Lett. **110,** 085504 (2013).
[3] Y. Feng *et al.*, Proc. Natl. Acad. Sci. U.S.A. **113,** 14656 (2016).
[4] L. Tao, E. Cinquanta, D. Chiappe, C. Grazianetti, M. Fanciulli, M. Dubey, A. Molle, and D. Akinwande, Nat. Nanotechnol. **10,** 227 (2015).
[5] W. F. Tsai, C. Y. Huang, T. R. Chang, H. Lin, H. T. Jeng, and A. Bansil, Nat. Commun. **4,** 1500 (2013).
[6] D. Solonenko, O. D. Gordan, G. L. Lay, H. Şahin, S. Cahangirov, D. R. T. Zahn, and P. Vogt, 2D Mater. **4,** 015008 (2016).
[7] J. C. Zhuang *et al.*, Phys. Rev. B **91,** 161409 (2015).
[8] A. Díaz Álvarez, T. Zhu, J. P. Nys, M. Berthe, M. Empis, J. Schreiber, B. Grandidier, and T. Xu, Surf. Sci. **653,** 92 (2016).
[9] M. Liao, S. Jiang, C. Hu, R. Zhang, Y. Kuang, J. Zhu, Y. Zhang, and Z. Dong, Nano Lett. **16,** 4040 (2016).
[10] R. Zhang *et al.*, Nature (London) **498,** 82 (2013).
[11] S. Jiang, Y. Zhang, R. Zhang, C. Hu, M. Liao, Y. Luo, J. Yang, Z. Dong, and J. G. Hou, Nat. Nanotechnol. **10,** 865 (2015).
[12] S. Baroni, S. de Gironcoli, A. Dal Corso, and P. Giannozzi, Rev. Mod. Phys. **73,** 515 (2001).
[13] G. Kresse and J. Hafner, Phys. Rev. B **47,** 558 (1993).
[14] D. Alfè, Comput. Phys. Commun. **180,** 2622 (2009).
[15] H. J. Monkhorst and J. D. Pack, Phys. Rev. B **13,** 5188 (1976).
[16] D. Chiappe, C. Grazianetti, G. Tallarida, M. Fanciulli, and A. Molle, Adv. Mater. **24,** 5088 (2012).
[17] P. Vogt, P. De Padova, C. Quaresima, J. Avila, E. Frantzeskakis, M. C. Asensio, A. Resta, B. Ealet, and G. Le Lay, Phys. Rev. Lett. **108,** 155501 (2012).
[18] B. J. Feng, Z. Ding, S. Meng, Y. Yao, X. He, P. Cheng, L. Chen, and K. Wu, Nano Lett. **12,** 3507 (2012).
[19] E. Scalise, M. Houssa, G. Pourtois, B. van den Broek, V. Afanas'ev, and A. Stesmans, Nano Res. **6,** 19 (2013).
[20] E. Cinquanta, E. Scalise, D. Chiappe, C. Grazianetti, B. van den Broek, M. Houssa, M. Fanciulli, and A. Molle, J. Phys. Chem. C **117,** 16719 (2013).
[21] See Supplemental Material at http://link.aps.org/supplemental/10.1103/PhysRevLett.119.196803 for detail analysis of the TERS enhancement factor and spatial resolution, and the vibration schematic for each Raman mode.
[22] B. Pettinger, B. Ren, G. Picardi, R. Schuster, and G. Ertl, Phys. Rev. Lett. **92,** 096101 (2004).
[23] N. Jiang *et al.*, Nano Lett. **12,** 5061 (2012).
[24] B. Pettinger, P. Schambach, C. J. Villagomez, and N. Scott, Annu. Rev. Phys. Chem. **63,** 379 (2012).
[25] J. Steidtner and B. Pettinger, Phys. Rev. Lett. **100,** 236101 (2008).
[26] J. Stadler, T. Schmid, and R. Zenobi, Nano Lett. **10,** 4514 (2010).
[27] J. Stadler, T. Schmid, and R. Zenobi, Nanoscale **4,** 1856 (2012).
[28] H. K. Wickramasinghe, M. Chaigneau, R. Yasukuni, G. Picardi, and R. Ossikovski, ACS Nano **8,** 3421 (2014).
[29] K. F. Domke, D. Zhang, and B. Pettinger, J. Am. Chem. Soc. **128,** 14721 (2006).
[30] R. M. Stockle, Y. D. Suh, V. Deckert, and R. Zenobi, Chem. Phys. Lett. **318,** 131 (2000).
[31] E. D. Palik, *Handbook of Optical Constants of Solids* (Academic Press, Orlando, 1985).
[32] N. L. Gruenke, M. F. Cardinal, M. O. McAnally, R. R. Frontiera, G. C. Schatz, and R. P. Van Duyne, Chem. Soc. Rev. **45,** 2263 (2016).
[33] P. Kukura, D. W. McCamant, and R. A. Mathies, Annu. Rev. Phys. Chem. **58,** 461 (2007).
[34] D. Solonenko, O. D. Gordan, G. Le Lay, D. R. T. Zahn, and P. Vogt, Beilstein J. Nanotechnol. **8,** 1357 (2017).
[35] J. L. Qiu, H. Fu, Y. Xu, A. I. Oreshkin, T. Shao, H. Li, S. Meng, L. Chen, and K. Wu, Phys. Rev. Lett. **114,** 126101 (2015).
[36] W. B. Li, S. X. Sheng, J. Chen, P. Cheng, L. Chen, and K. Wu, Phys. Rev. B **93,** 155410 (2016).